Proceedings of the CAS–CERN Accelerator School: Beam Injection, Extraction and Transfer, Erice, Italy, 10-19 March 2017, edited by B. Holzer, CERN Yellow Reports: School Proceedings, Vol. 5/2018, CERN-2018-008-SP (CERN, Geneva, 2018)

Magnets and Special Magnets

C. Muehle
GSI Helmholtz Centre for Heavy Ion Research, Darmstadt, Germany

Abstract
Magnets are key components of all charged particle accelerators, their beam lines, and their experiments. They are used to guide, focus, and correct charged particle beams. Depending on the varying requirements of different accelerators, the simple underlying physics leads to a wide variety of types and designs.

Keywords
Accelerator magnets; dipoles; quadrupoles; sextupoles; steering magnets.

1 Introduction

This paper is intended as a brief introduction to the normal conducting accelerator magnets. Their basic physics along with the underlying principles of magnet design and technical realization are discussed and presented here. The aim is to provide a general understanding on the basis of first principles and very simple calculus.

The second chapter gives a brief introduction into the basic physics. The third chapter describes magnet types, their influence on the charged particles, as well as technical issues such as polarity and design types. The fourth chapter concentrates on coils. Methods for the estimation of excitation currents are derived, conductor materials are compared, and cooling as well as coil shapes are explained. Chapter five is dedicated to yokes. Yoke materials are compared, and saturation effects and their corresponding countermeasures are explained. Special magnets are the topic of chapter 6. Magnets that are special with respect to design features or materials, as well as magnets which cannot be described by multipoles, are illustrated here. Examples are directly integrated. Chapter 7 describes examples of standard accelerator magnets. This is elucidated with the magnets used for the cancer therapy accelerator Heidelberg Ion-beam Therapy Center (HIT), in Heidelberg.

2 Basic physics

2.1 The Lorentz force

Charged particles experience forces when subjected to electric or magnetic fields. The force exerted by an electromagnetic field on them is given by the Lorentz force[1] as in Eq. (1)

$$\vec{F} = q\left[\vec{E} + \left(\vec{v} \times \vec{B}\right)\right], \qquad 1)$$

where, q is the charge of the particle, $\vec{E}$ is the electric field, $\vec{v}$ is the velocity of the charged particle, and $\vec{B}$ is the magnetic flux density.

[1] The first derivation of the Lorentz force is commonly attributed to Oliver Heaviside in 1889, although other historians suggest an earlier origin in an 1865 paper by James Clerk Maxwell. Hendrik Antoon Lorentz derived it in 1895, a few years after Heaviside. (Wikipedia)

https://doi.org/10.23730/CYRSP-2018-005.193

2.2 Maxwell's equations

Maxwell's equations[2] are a collection of laws governing electromagnetism. Writing them in the differential and integral forms using SI convention yields the equations in Table 1.

Table1: Maxwell equations

Law	Differential form	Integral form
Gauss's law for electrostatics	$\nabla \cdot D = \rho$	$\oint_{\partial v} D \cdot \mathrm{d}A = Q$
Gauss's law for magnetism	$\nabla \cdot \mathrm{B} = 0$	$\oint_{\partial \mathrm{v}} \mathrm{B} \cdot \mathrm{dA} = 0$
Faraday's law of induction	$\nabla \times \mathrm{E} = -\frac{\partial \mathrm{B}}{\partial \mathrm{t}}$	$\oint_{\partial \mathrm{A}} \mathrm{E} \cdot \mathrm{ds} = -\frac{\mathrm{d}}{\mathrm{dt}} \int_{\mathrm{A}} \mathrm{B} \cdot \mathrm{dA}$
Ampere's circuital law	$\nabla \cdot H = j + \frac{\partial D}{\partial t}$	$\oint_{\partial A} H \cdot \mathrm{d}s = \int_{A} j \cdot \mathrm{d}A + \frac{\mathrm{d}}{\mathrm{d}t} \int_{A} D \cdot \mathrm{d}A$

The differential formulation serves to provide a basic understanding between the physical quantities and their nature while the integral form comes in handy when actually performing calculations to quantify the terms. In the context of this report, only Gauss's law for magnetism and Ampere's circuital law are of interest. The first forbids the existence of magnetic monopoles. The latter will be used for the calculation of excitation currents.

2.3 Magnetic material properties

The defining equation of a magnetic material is given by the relation,

$$B = \mu H \,, \tag{2}$$

with $\mu = \mu_0 \mu_r$.

The structure and physical properties of magnetic materials are defined by the concepts of isotropy and homogeneity [1].

(i) When μ is a constant number, the material is a *simple magnetic material.*

(ii) When μ varies according to the position in a material as $\mu(r)$, it is an *inhomogeneous magnetic material.*

(iii) When μ becomes a function of H, as in $\mu(H)$, B and H are no longer proportional, thus defining a *non-linear magnetic material.*

(iv) When the relation between B and H becomes highly non-linear such that μ cannot be clearly defined, it is a *ferromagnetic material.*

(v) When μ is a tensor $\lfloor \mu \rfloor$, it yields $B = \lfloor \mu \rfloor . H$. This means that B and H have different directions making it an *anisotropic material*. Under specific rotations, $\lfloor \mu \rfloor$ transforms as a second rank tensor usually called the permeability tensor given by,

[2] The four modern Maxwell's equations can be found individually throughout his 1861 paper, derived theoretically using a molecular vortex model of Michel Faraday's "lines of force" and in conjunction with the experimental result of Weber and Kohlrausch. But it wasn't until 1884 that Oliver Heaviside, concurrently with similar work by Josiah Willard Gibbs and Heinrich Hertz, grouped the twenty equations together into a set of only four, via vector notation. This group of four equations was known variously as the Hertz–Heaviside equations and the Maxwell–Hertz equations, but are now universally known as Maxwell's equations. Heaviside's equations, which are taught in textbooks and universities as Maxwell's equations are not exactly the same as the ones due to Maxwell, and, in fact, the latter are more easily forced into the mould of quantum physics. (Wikipedia)

$$\mu = \begin{bmatrix} \mu_{xx} & \mu_{xy} & \mu_{xz} \\ \mu_{yx} & \mu_{yy} & \mu_{yz} \\ \mu_{zx} & \mu_{zy} & \mu_{zz} \end{bmatrix}. \quad (3)$$

Different combinations of properties and their influence on the permeability tensor are compiled in Table 2.

Table 2: Overview of material types

Material	Tensor terms
Isotropic and homogeneous	$\mu_{ij} = 0, \mu_{ii} = \mu_r \neq 0$
Isotropic and inhomogeneous	$\mu_{ij} = 0, \mu_{ii} = \mu_r(x, y, z)$
Anisotropic and homogeneous	$\mu_{ii} = constant$
Anisotropic and inhomogeneous	$\mu_{ij} = constant, \mu_{ii} = \mu_r \neq 0$
Isotropic, homogeneous, nonlinear (massive iron)	$\mu_{ij} = 0, \mu_{ii} = \mu_r(\vec{H}(x, y, z))$
Anisotropic, homogeneous, nonlinear (laminated iron)	$\mu_{ij} = \mu_{ij}(\vec{H}(x, y, z))$

3 Magnet types

3.1 Magnets in the accelerator

Magnets in accelerators can be basically subdivided into three groups – namely bending magnets, focussing magnets, and non-linear magnets.

Bending magnets are dipoles. With a constant magnetic field across the aperture, they deflect charged particle beams along a curved path.

Focussing magnets are quadrupoles. The magnetic field increases linearly starting from zero on the axis (from the centre of the magnet). It can therefore be expressed by a gradient.

Non-linear magnets exhibit a non-linear increase in the magnetic field starting from zero on the axis (from the centre of the magnet). The most common ones are sextupoles and octupoles. These magnets are used as corrector magnets.

These magnets are sketched in Fig. 1.

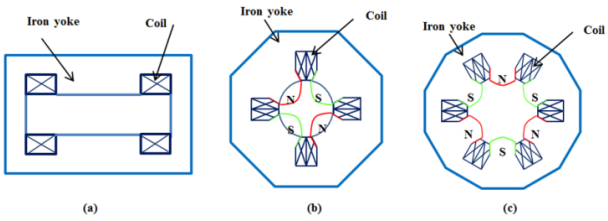

Fig. 1: (a) H-type dipole (b) quadrupole (c) sextupole

3.2 Optics analogies

The influence of the magnets on the beam can be easily shown by taking a look at their respective optical analogies, as seen in Fig. 2.

The optical analogy of a dipole is the prism. The incident beam is deflected by a certain angle.

Spherical lenses are analogous to quadrupoles. The focussing or defocussing is independent of the distance to the axis.

Aspherical lenses have the same behaviour as non-linear magnets. The strength of the focussing or defocussing is dependent on the distance to the axis.

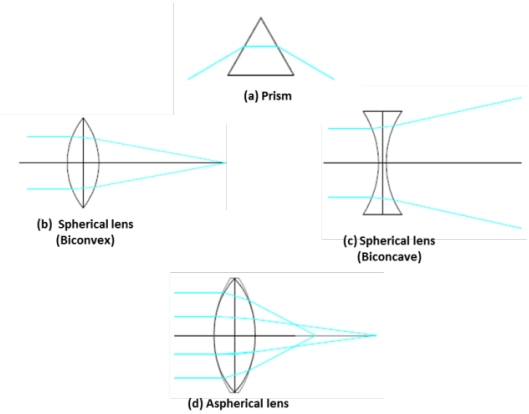

Fig. 2: (a) Illustration of a deflecting dipole (b) illustration of a focussing quadrupole (c) illustration of a defocussing quadrupole (d) illustration of non-linear magnets with dependence on the focal length.

3.3 Magnetic flux lines

The topology of the magnetic field can be visualized by plotting the equipotential flux lines, as seen in Fig. 3. Higher order multipoles follow the same pattern.

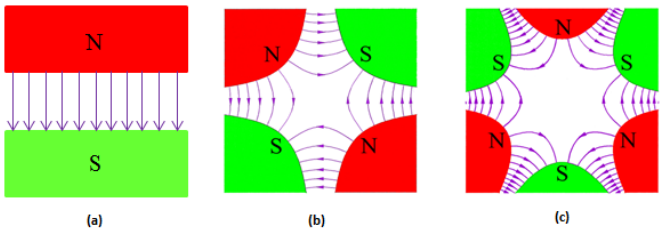

Fig. 3: (a) Dipole – parallel and equidistant lines, (b) quadrupole – radially symmetric lines with alternating directions (four poles), and (c) sextupole – radially symmetric lines with alternating directions (six poles).

3.4 Definition of conventions

The direction of the magnetic field ($\vec{B}$) in an electromagnet is determined by the direction of the current ($\vec{I}$) in its coils. To understand the orientations of $\vec{B}$ and the flux ($\vec{\Phi}$) due to $\vec{I}$, we use the right-hand rule as a tool. This rule provides the relation between these vectors in the positive direction (counter clockwise). By convention, it is taken that the positive current flows from the positive terminal of the power supply to the negative terminal. This is defined as the conventional current direction, which incidentally is the same for a positively charged ion. In the similar way, the polarity of the magnet is defined by the magnetic flux flowing from the north pole to the south pole of a magnet.

If the fingers envelope the coil with the finger tips pointing in the direction of the current, the thumb indicates the direction of the magnetic field as seen in Fig. 4.

Fig. 4: Right-hand rule to find the direction of the magnetic field in a coil

Applying the above discussions to our magnets, we can find the direction of *B* using the first part of the right-hand rule as follows:

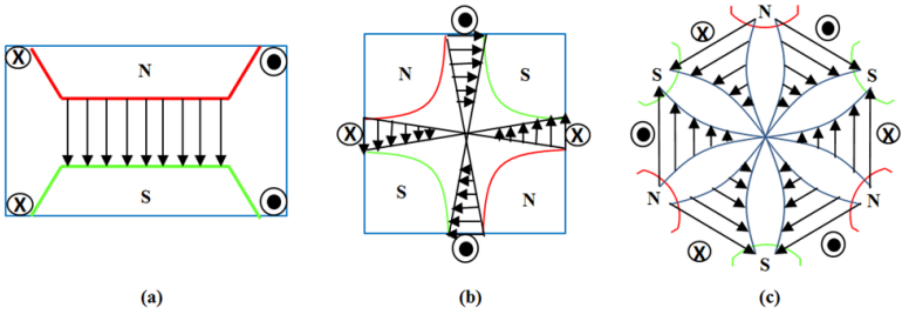

Fig. 5: Magnetic field direction in different magnets in dependence of the current direction in the coils: (a) dipole, (b) quadrupole, and (c) sextupole. '⊗' indicates positive current into the paper while '⊙' indicates positive current out of the paper.

3.5 Forces on the charged particle beam

As the force on a charged particle in a magnetic field is defined by the cross product, as in Eq. (1), the deflection can easily be found using the second part of the right-hand rule. To find the direction of the force exerted on the charged particle, point the thumb along the direction of movement of the charge. With the pointer finger along the direction of the magnetic field, the middle finger indicates the direction of force experienced by the particle.

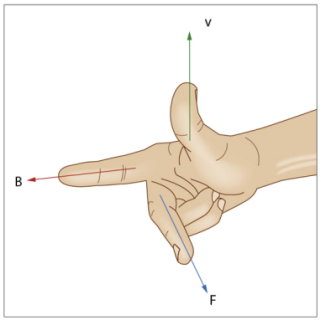

Fig. 6: Right-hand rule to find the force exterted on a charged particle

Due to the constant field in a dipole, a constant force can be found in the aperture. Figure 7, shows the force exerted by the field on a positive ion flying into the plane. It is bent to the left.

The force in a quadrupole follows the characteristic behaviour of its magnetic field (linear dependence). As the direction of the magnetic field alternates, the same is observed with the force too. In the example shown in Fig. 7, the positive ion beam is bent in the vertical plane towards the axis and away in the horizontal plane. This effect focusses the beam in the vertical plane and defocusses it in the horizontal plane. The naming convention is based on the effect in the horizontal plane. In this case

we have a defocussing quadrupole. A net focussing in both planes can only be achieved by using more than one quadrupole. A formation of two or three quadrupoles is called doublet or triplet respectively.

In a sextupole however, the magnetic field increases quadratically with the distance from the axis. The same is valid for the modulus of the force. But now we have a sixfold symmetry. Hence, we have three distinguished planes namely the median plane (along the horizontal axis) and two other planes at 120° azimuth and 240° azimuth respectively. The force now has the same direction on both sides of the median axis. Naming can be done now only with respect to the complete machine. If bending is towards the centre of a circular machine, the sextupole is called a focusing one.

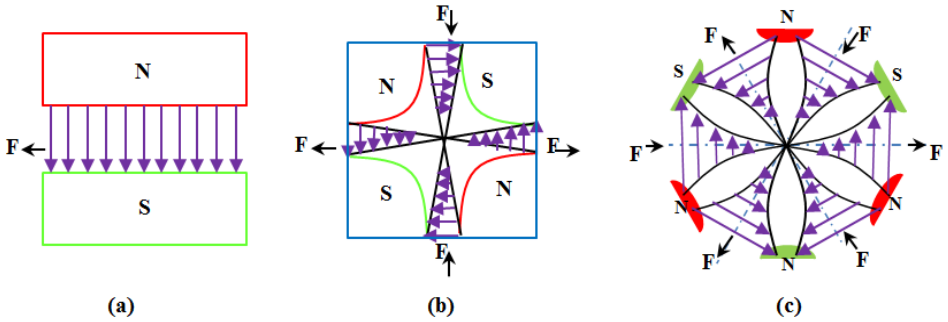

Fig. 7: Force direction in different magnets for a positive beam flying into the plane. (a) Dipole, (b) defocussing quadrupole, and (c) sextupole.

3.6 Design types

Magnets can be distinguished according to the effects dominating their field quality. The field distribution can either be current dominated or iron dominated.

Current dominated magnets are classified according to their coil shape. Typical representatives of current dominated dipoles are the $\cos n\theta$ magnets and intersecting ellipses (see Fig. 8). As our discussion is limited to the iron-dominated magnets alone, we do not discuss the current-dominated type magnets further.

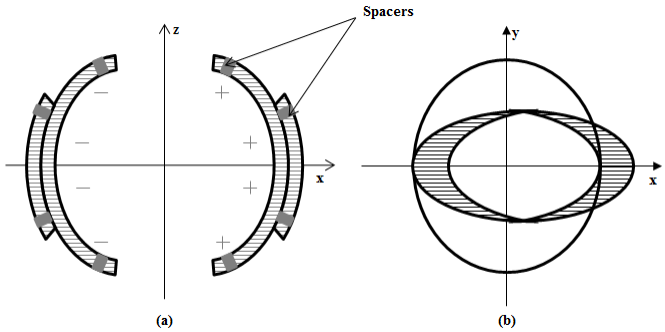

Fig. 8: Current dominated magnets: (a) $\cos n\theta$ dipole (b) dipole formed by crossed ellipses

Iron-dominated magnets are classified according to their yoke shapes. This is separately discussed further in sub sections 3.6.1 and 3.6.2 for dipoles and quadrupoles respectively.

3.6.1 Dipole types

Iron-dominated dipole magnets are classified according to their yoke shapes as the window-frame magnet and C-type magnet, or according to the shape of the aperture including the coil windows as H-type magnet (see Fig. 9). The coils are indicated in red. According to their yoke shape, the magnets exhibit different advantages and disadvantages.

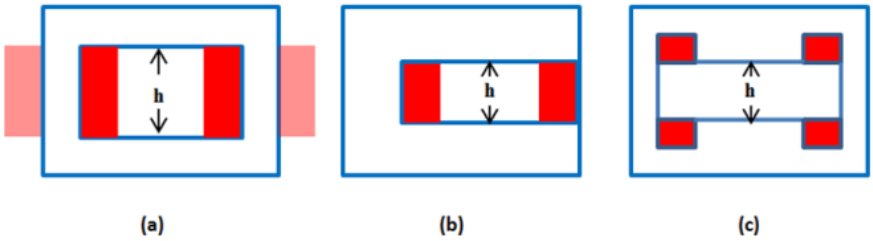

Fig. 9: Yoke shapes of iron dominated dipoles: (a) window-frame or O-type magnet, (b) C-type magnet, (c) H-type magnet.

The window-frame type has the most symmetric design. It can either be equipped with complex bedstead coils or cylindrical coils creating a higher leakage flux. Cylindrical coils are typically only used for short magnets, e.g., correction dipoles (so called steering magnets).

The C-type magnet saves space on one side of the yoke at the cost of an enlargement with an increased thickness above and below the poles in comparison to the window-frame magnet. As can be seen in Fig. 9, the same overall size gives a much smaller gap height for the C-type magnet in comparison to the window-frame magnet.

The H-type magnet has again the advantage of a symmetric design. The coils are simple to manufacture as they are flat. They have a so-called racetrack design. The comparison is compiled in Table 3.

Table 3: Comparison between iron-dominated dipole shapes

Magnet	Advantages	Disadvantages
Window frame type (O-type)	Symmetrical design	Bedstead coils or cylindrical coils with high flux leakage
C-type	Saves space on one side of the yoke, simple coil assembly	Asymmetrical, bedstead coil, heavy yoke
H-type	Symmetrical design, simple racetrack coils	Bad field quality (compared to window frame)

The field quality of the designs can be compared by using the orthogonal analogue model [2]. At first, 'flow' lines from plus to minus currents are drawn. The field lines are orthogonal to the flow lines and end perpendicularly at the iron boundaries (see Fig. 10).

The window-frame type shows a perfect field quality if the coil window is vertically completely filled with the coil. In real cases this is limited due to the insulation of the coil.

In an H-type magnet the field quality decreases when horizontally moving from the centre of the magnet. This can be mitigated either by adding adequate shims to the pole corners or by enlarging the width of the pole.

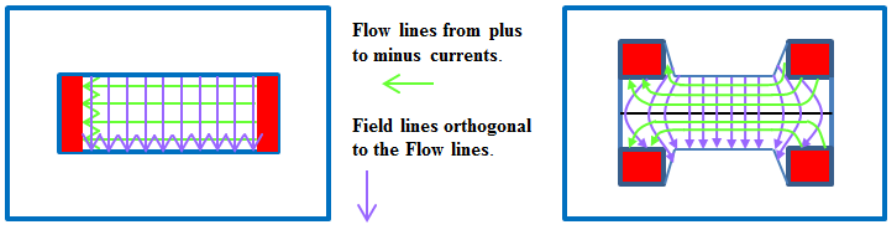

Fig. 10: Comparison of window-frame type and H-type dipoles with respect to their field quality

3.6.2 Quadrupole types

Iron-dominated quadrupoles exhibit a hyperbolic pole shape as seen in Fig. 11.

The Collins or figure of eight quadrupole is limited in width at the cost of additional height required for the yoke design. The upper and lower half of the yoke is magnetically decoupled.

The standard quadrupoles differ in their pole sides. The standard type I design has parallel sides. Therefore, the pole base has the same width as the pole itself. The standard type II design exhibits the largest possible increase in the pole base. The pole sides have an angle of 90° between each other. The type 1 has more space for simpler coils but tends to saturate inside the pole. Real quadrupoles are often hybrid designs of the above mentioned types.

The Panofsky quadrupole is a current dominated magnet shown here as an exception. The window-frame yoke collects the stray field and increases the field strength in the aperture. By using the orthogonal analogue method, one can convince oneself that this dipole-like looking magnet is a quadrupole.

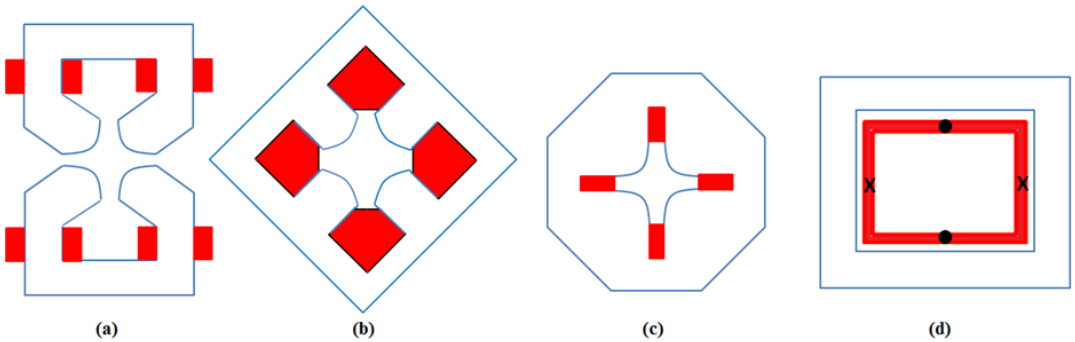

Fig. 11: Yoke shapes of quadrupole types: (a) Collins or figure of eight quadrupole, (b) standard quadrupole type I, (c) standard quadrupole type II, (d) Panofsky quadrupole.

4 Coils

4.1 Ampère's law

Ampère's law enables us to calculate the necessary excitation current in a magnet coil. The law states that (Eq. (4)),

$$\oint_{\partial A} H \cdot \mathrm{d}s = \int_A j \cdot \mathrm{d}A + \frac{\mathrm{d}}{\mathrm{d}t}\int_A D \cdot \mathrm{d}A\,.$$

Neglecting the time-dependent part, the closed loop integral over the magnetic field equals the enclosed current.

4.2 Dipole excitation

We are now going to execute the integration in Eq. (4) for a dipole. Figure 12 illustrates the following steps.

Starting at the centre of the magnet, we integrate at first the vertical air path in the gap. The path is parallel to the field direction and μ_r equals one.

$$\int \frac{\vec{B}}{\mu_0\mu_r}.\vec{\mathrm{d}l} = \frac{Bh}{\mu_0}.$$

Secondly, we do the integration through the iron yoke. The expression

$$\int \frac{\vec{B}}{\mu_0 \mu_r} . \vec{\mathrm{d}l} = \frac{Bh}{\mu_0 \mu_r} ,$$

gets small as μ_r is large.

Finally, we integrate the horizontal path. As $\vec{B}$ and $\vec{l}$ are perpendicular to each other we get

$$\int \frac{\vec{B}}{\mu_0 \mu_\mathrm{r}} . \vec{\mathrm{d}l} = 0 .$$

Summing up and taking into account that the enclosed current equals number of turns in one coil times the current in it, we get

$$NI_\mathrm{dipole} \approx \frac{Bh}{\mu_0} .$$

The expression NI is often called *ampere turns*.

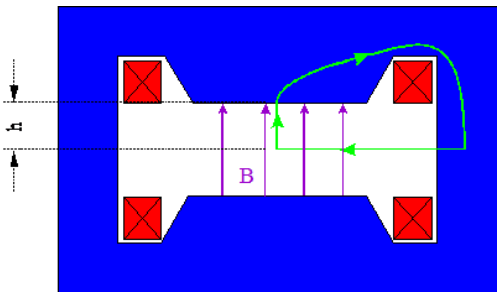

Fig. 12: Calculation of the excitation current in a dipole with the help of Ampere's law. The used integration path is shown in green.

4.3 Quadrupole excitation

The very same scheme can be used for quadrupoles, too. Again we start at the centre of the aperture. Exploiting the symmetry, we calculate for ¼th of the magnet as in Fig. 13. The path in the aperture is parallel to the field direction and μ_r equals one. We integrate a linearly increasing field represented by its gradient B' and get,

$$\int \frac{\vec{B}}{\mu_0 \mu_\mathrm{r}} . \vec{\mathrm{d}l} = \int_0^{r0} \frac{B'l}{\mu_0 \mu_\mathrm{r}} \mathrm{d}l = \frac{B' r_0^2}{2\mu_0} .$$

The integral through the iron yoke is again small as μ_r is large.

The integral along the horizontal path is again zero as $\vec{B}$ and $\vec{l}$ are perpendicular to each other.

Summing up we get,

$$NI_\mathrm{quadrupole} \approx \frac{B' 2 r_0^2}{2\mu_0}$$

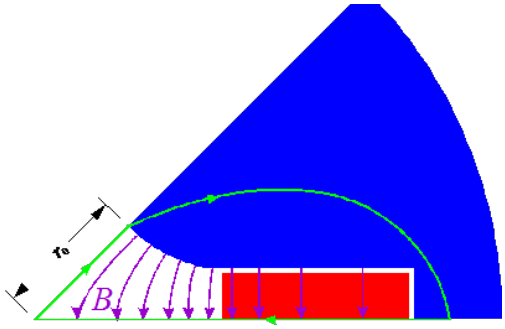

Fig. 13: Calculation of the excitation current in a quadrupole with the help of Amperes law. The used integration path is shown in green.

The very same procedure can be used for sextupoles too. This yields the ampere turns to be:

$$NI_{\text{sextupole}} \approx \frac{B'' r_0^3}{6\mu_0}.$$

4.4 Conductor materials

The power consumption of a magnet is given by the conductivity of its conductor material. Therefore, high conductivity copper and pure aluminium are used. Their different properties make them potential candidates for typical applications (see Table 4).

At a first glance, copper is the better choice due to its 1.6 times higher conductivity and smaller oxidation in comparison to aluminium. But, the weight price of copper is three to four times more than that of aluminium. Additionally, copper has three times the density of aluminium.

However, the co-efficient of thermal expansion of both materials lie in a comparable range among other physical properties between the two. The elasticity modulus of copper is about 1.7 times larger. Also, the deformation of the conductor cross-section while using small bending radii is larger for copper. This effect is called key stoning, as the square cross-section is deformed to a trapezoidal like shape (as seen in Fig. 14) similar to the keystone in the roman arch.

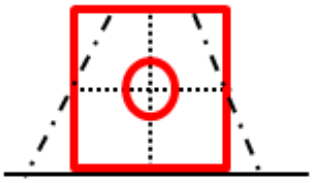

Fig. 14: Keystone effect in a copper conductor with cooling duct showing the deformation of a square conductor into a trapezoidal shape.

For the same amount of ampere turns we can conclude the following: Copper allows us to build smaller but heavier coils. Due to the higher density, the transparency for particles is smaller than for aluminium. The investment costs are higher. However, the operating costs are smaller as the conductivity is larger. Therefore, an application with a long annual operational period is favourable. This is typical for accelerators and their corresponding beam lines.

On the contrary, detector magnets have typically shorter annual operational periods. While using aluminium in this case, it is an advantage as this leads to lower investment costs. In addition, it can be used for detecting particles that have passed through the coil as the lower material density of aluminium enables this.

In any case, mixing of copper and aluminium coils inside one cooling circuit must be avoided. Otherwise, the aluminium coil would act as a sacrificial anode in perspective of a long-term operation.

Table 4: Comparison of the properties of aluminium and copper

Property	**Aluminium (pure, > 99.5%)**	**Copper (OFHC- oxygen free high conductivity)**
Conductivity	36 S m/mm^2	58 S m/mm^2
Oxidation	In air: AlO layer is formed. Dissolves in mixed copper/ aluminium cooling circuits.	Small
Price (large quantities)	2.7−3.4 EUR/kg	8−16 EUR/kg
Specific weight	2.70 g/cm^3	8.96 g/cm^3
Linear expansion coefficient	23 ×10^{-6} K^{-1}	17 × 10^{-6} K^{-1}
Elasticity modulus	72,000 N/mm^2	123,000 N/mm^2
Key stoning effect	Smaller	Higher
Conclusions	Larger coils are needed	Smaller coils are needed
(for same N × I)	Lighter	Heavier
	Higher transparency[3] for particles	Reduced transparency for particles
	Lower investment costs	Higher investment costs
	Higher operating costs	Lower operating costs
	⇨ Better suited for detector magnets	⇨ Better suited for accelerator magnets

4.5 Coil cooling

The power produced in the coils during operation has to be dissipated to avoid overheating. Typical media for cooling are air and water.

Air cooling is limited to low-power applications as the heat capacity is smaller than that for water. In the case of free flow, the cooling is based on convection. If this is not sufficient, forced flow air cooling can be provided by fans.

The most common method is direct water cooling with hollow conductors. The water is in direct contact with the conductor and provides efficient cooling. For low-current (high turn) applications, the conductor cross-section becomes too small to incorporate an internal cooling channel. In this case, separate water cooled radiators are used. An example with cooling discs [4] is shown in Fig. 15.

[3] The stopping of particles depends on the number of protons in the nucleus of the metal. For detector magnets, a low stopping power of materials (= high transparency) is of interest.

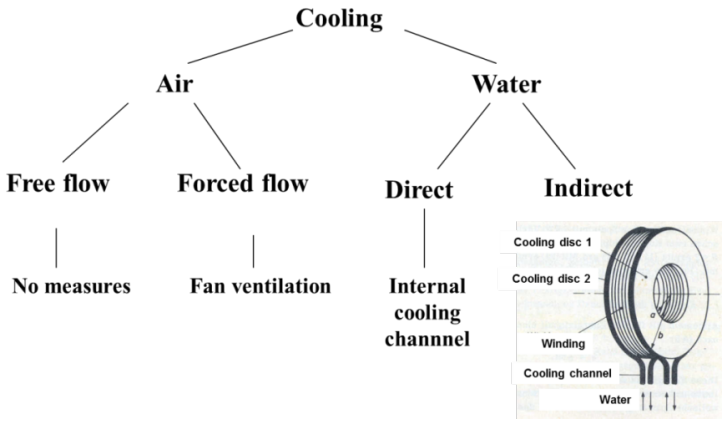

Fig .15: Cooling methods for normal conducting magnets

4.6 Conductor profiles

Wide variety of hollow copper conductors are commercially available (refer to Fig. 14). The most common shapes are the quadratic or rectangular conductors with a round cooling channel. These conductors allow good packing factors in the coil cross-section. Bending radii smaller than three to five times the cross-section should be avoided because of the keystone effect and rupture problems.

Round conductors are used in the case of small coils with tight bends in several directions. Examples are quadrupoles and steering magnets.

Fig. 16: Examples of hollow copper conductors [3]

4.7 Coil shapes

The coil shape is determined by the (yoke) design type. Besides supplying the needed ampere turns, it has to fit to the yoke and must not interfere with the beam aperture.

When recalled from section 3.6.1, H-type dipole magnets have simple flat coils. They are called cylindrical or racetrack coils as in Fig. 17 (c).

For window-frame magnets, either cylindrical or bedstead coils can be used. In case of cylindrical coil, it is wound around the yoke. This increases the stray fields around the magnet. Additionally, the coil circumference is increased to more than double the magnet length per coil. Therefore, cylindrical coils are only used in short magnets, like steering magnets. While using bedstead coils however, additional care must be taken such that the coil ends for long window-frame

magnets be cranked, to keep the beam aperture free. In this case they resemble Fig. 17 (a) or (b) and are named saddle or bedstead coils.

To sum up, the most commonly used coil for window-frame dipoles is the bedstead type. Racetrack coil is used only in cases where the overall magnet length has to be limited.

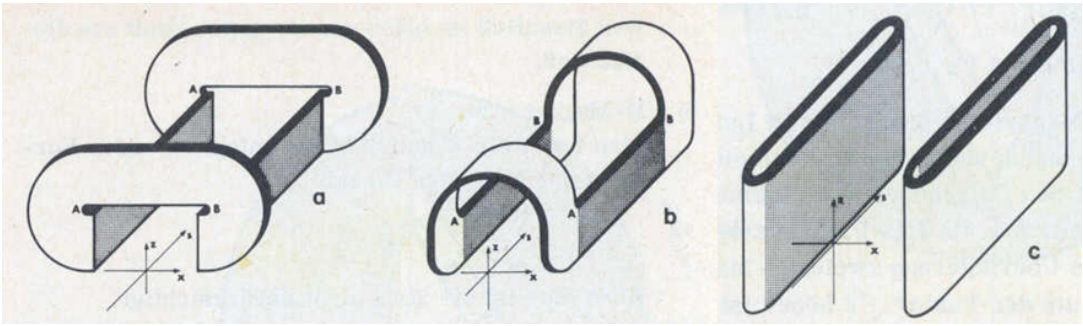

Fig. 17: Coil types for dipole magnets [4]: (a) saddle or bedstead coil with horizontal bend, (b) saddle or bedstead coil with a vertical bend. For (a) and (b) only the upper part is shown. (c) Cylindrical or racetrack coil. A pair is used in (short) window-frame magnets. One cylindrical coil per pole is used in H-type magnets.

A similar classification can be done for quadrupole magnets too. The coils for figure of eight quadrupoles and standard quadrupoles of type I have cylindrical coils. The coils for standard quadrupoles of type II need to have cranked ends. They are similar to the bedstead coils in Fig. 17 (a).

4.8 Coil potting

To form a rigid coil body and to maintain the insulation properties over long periods, a process known as coil potting is to be performed. Initially, the conductors of standard coils are wrapped with glass fibre tapes with half overlap during winding. The final coil body is then wrapped again with the same for ground insulation. Next, it is vacuum impregnated with an epoxy resin. Depending on the requirements, dedicated precision moulds for single coils or large common moulds for several coils are used. Finally, the coil body is often wrapped with a mould release film before potting as this eases the removal of the excess epoxy resin after the potting process.

5 Yoke

5.1 Yoke materials

All yoke materials (ferromagnetic in nature) exhibit a nonlinear relationship between the magnetic flux density and the magnetic field strength (H) given by the equation,

$$B = \mu(H)H,$$

with $\mu = \mu_0\mu_r$.

This behaviour is depicted in the B-H curves (see Fig. 18). A high relative permeability μ_r is always desirable as this guarantees the flux guiding function of the yoke.

Most commonly used is the so called soft iron which has high purity in iron content (low carbon). Saturation starts at about 1.5 T. Higher saturation flux densities can be reached by adding up to 50% of cobalt.

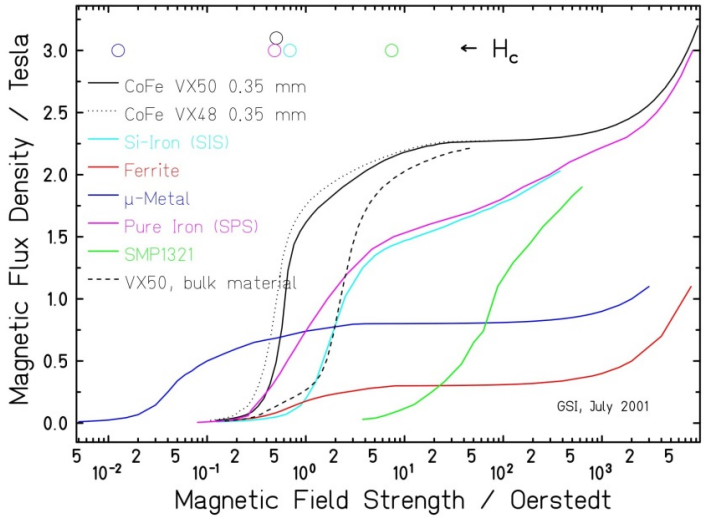

Fig. 18: Compilation of *B-H* curves for typical yoke materials. For comparison, μ-metal is shown too. It has very high permeability at low fields and is therefore used for screening at low fields.

In non-DC applications, the conductivity of the yoke material must be taken into account. The time varying fields generate eddy currents in the yoke. These currents can be limited by increasing the electrical resistance of the yoke. The basic measure is to use a laminated yoke instead of a massive one. In this case, the yokes are stacked from thin plates as in a transformer. Also, the resistance of iron can be increased by adding up to ~4% silicon to it. If this is not sufficient, sintered iron or ferrites can even be used. Unfortunately, with all these measures the permeability is reduced.

The final choice of the yoke material is therefore determined by the required flux density and the ramp rate, as well as the space requirements and material costs (as seen in Fig. 19).

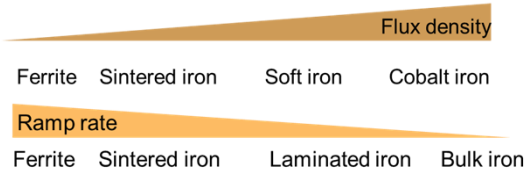

Fig. 19: Suitability of different yoke materials with respect to flux density and ramp rate

5.2 Saturation effects

As described above, the saturation for soft iron starts at about 1.5 T. This means, that μ gets smaller for flux density levels above 1.5 T. The flux density level as well as the field quality is influenced by this effect (summarized in Fig. 20).

In comparison to the equations derived in section 4.2 and 4.3, the field level gets smaller as the assumption of a large μ is not valid anymore. This effect is named *ampere turn loss*. This can be compensated either by increasing the ampere turns or by adapting the yoke design accordingly. The yoke design can be adapted by either increasing the width of the yoke or using a material with higher saturation flux density.

On the other hand, reduced field quality is caused by non-homogenous spatial distribution of saturation in the yoke. One countermeasure is to adapt the pole profile by mainly increasing the pole

width, thus moving the regions with reduced field quality further away from the region of interest. The second method is an active correction of the field quality by using the so called *pole face winding*. They act as a superimposed current dominated correction magnet. The third method is to introduce air slits in the poles (shown in Fig. 21). In H-type dipoles, they aim on equalizing the spatial distribution of saturation. The slits are located at the pole centre where the saturation is small. Due to the reduced iron, the areas around the holes tend to saturate at lower field levels and the effect of saturation is homogenized across the yoke. However, the consequence of this method is a further loss of ampere turns. In window-frame dipoles, the holes are positioned on the sides of poles (indicated in Fig. 22). For higher fields, these parts of the poles are switched off. The flux lines have to then go around the holes and the flux close to the pole is equalized, thus leading to an improved field quality.

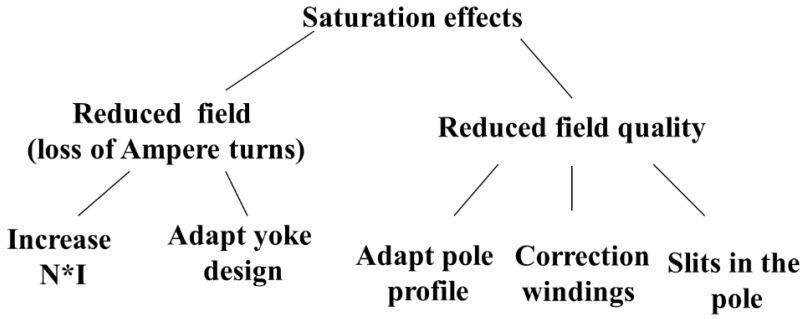

Fig. 20: Consequences of saturation and its countermeasures

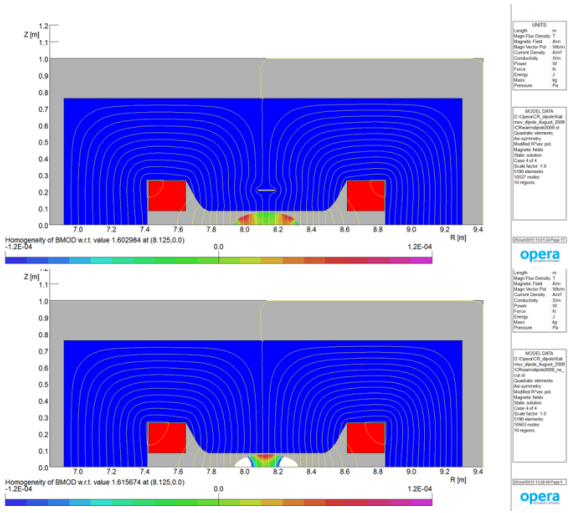

Fig. 21: Methods to minimize the influence of saturation on the field quality: H-type dipole with holes in the centre of the pole.

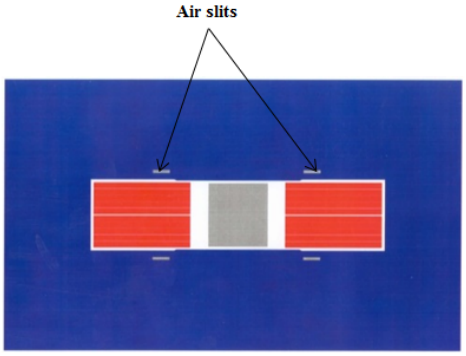

Fig. 22: Methods to minimize the influence of saturation on the field quality: window-frame type dipole with slits on the sides of the pole.

5.3 Curved yokes

As the beam describes a circular path inside the magnet, the sagitta 'h' comes into play. It depends on the radius r and the deflection angle α and is proportional to the square of the magnet length l.

$$h = r \cdot (1 - \cos(\alpha/2)) \propto l^2 .$$

Building a straight dipole is much simpler and therefore less costly than a curved one. But a wider aperture needs to be provided which increases the magnet's cross-section and is a cost driver too.

If a straight magnet is rotated by half of its deflection angle with respect to the incoming beam and shifted by half of the sagitta, its aperture width is used most efficiently (illustrated in Fig. 23). In that case, the mechanical aperture of the magnet needs to be the sum of beam width and sagitta. The ratio of beam width to sagitta is used for deciding between straight and curved yokes.

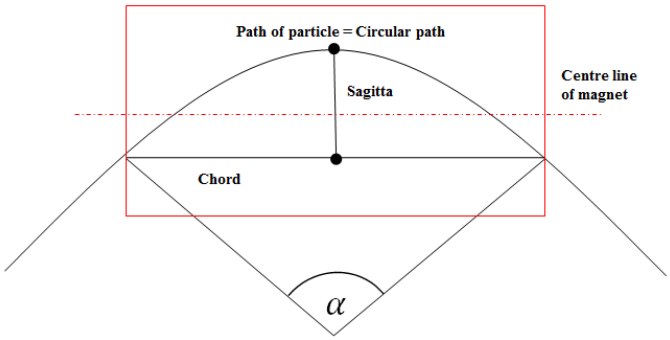

Fig. 23: Curved beam path in a straight dipole magnet

Laminated magnet yokes are typically stacked from fine blanked laminations. For curved magnets, they are stacked with their corresponding radii. Therefore, a curved stacked yoke has the same radii for the poles and back legs but different centres, whereas a massive yoke would have different radii but the same centre for all curved parts (depicted in Fig. 24). The useful aperture of a stacked yoke is therefore reduced in dependence of the deflection angle given by the reduced aperture,

$$b = a \cdot \cos\frac{\alpha}{2}.$$

To limit this effect, magnets with large bending angles are fabricated from several stacks. The ends of the individual stacks are cut under the appropriate angle and fixed together to one yoke.

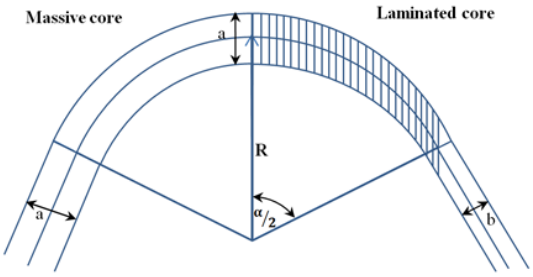

Fig. 24: Comparison of curved yokes: left side shows a massive yoke. All radii have the same centre. The useful aperture is hence constant. Right side shows a laminated yoke. All radii are identical but the centres are different. The useful aperture at the entrance of the magnet is reduced.

6 Special magnets

6.1 Introduction

In the following, two criteria will be used to distinguish special magnets from normal ones. The first are magnets with special features or materials in their designs. These are the following.

- Magnetic septa -> separate report by M. Paraliev.
- Kicker magnets -> separate report by M. Barnes.
- Radiation resistant magnets.
- Special yoke shapes.
- Integrated magnets.
- Magnets with cobalt iron yokes.
- ...

The other kind of special magnets are those which cannot be described by multipoles as shown in section 3.1. These are the following.

- Solenoids.
- Magnetic horns.
- Toroids.
- ...

6.2 Radiation resistant magnets

In accelerators, beam losses always occur that could either be intended or unavoidable. Intended beam losses occur on targets as well as during charge state separation or mass separation. Examples for unavoidable losses are charge exchange reactions on residual gas or electrical septum wires as well as resonances.

The material of the magnet must be chosen with respect to the expected radiation level and intended life time. The most sensitive component is typically the coil insulation.

Standard epoxy resins have radiation resistances of the order of 10^7 Gy. This can be increased by one order of magnitude by using improved plastics as polyimide or isocyanates. If even higher radiation resistances are required, a fully inorganic design must be chosen. A radiation resistance of more than 10^9 Gy can be realized.

Using improved plastics does not influence the conductor and coil design itself (Fig. 25). But the tooling for coil potting must be adapted to the different procedures. This can be for instance cooling of moulds for coil potting.

Fig. 25: Coils for an external beam line at KEK potted with improved plastics. At first glance no difference to standard coils is to be seen (photo K. H. Tanaka).

The fully inorganic solution requires a completely different design (as in Fig. 26). Metal oxide insulated conductors (MIC) are used for the coil. They consist of an inner copper part which carries the current. It is surrounded by a MgO-layer serving as insulator. The structure is held together by another copper sheath. This set-up requires much larger bending radii in comparison to standard copper conductors. Special care must be taken for joints and end caps as MgO is hygroscopic and its insulation properties are lost in humid condition. MIC are available as hollow conductors and without central bore. In high radiation fields, the combination of current and cooling water might lead to radiolysis. Then, MIC without bore holes are used and dedicated radiators are added to the coil structure. The complete coil structure is finally potted in solder.

Fig. 26: Radiation resistant dipole prototype for the SuperFRS pre-separator (photo G. Otto, GSI Darmstadt)

6.3 Special yoke shapes

External requirements may demand special yoke shapes. In most cases, these are limitations by surrounding beamlines and installations of the same accelerator, e.g., beam lines for injection and extraction as well as branching beam lines.

Most common are the C-shaped yokes of the magnetic septa (see separate report by M. Paraliev). But, standard H-type dipoles can also be re-designed to fit the requirements for branching points. Figure 27 shows the 45° high energy beam transport (HEBT) bending dipole for the cancer

therapy facility HIT in Heidelberg. This dipole is used to branch the beam to the different treatment areas. Its yoke has an opening to accommodate the straight beam pipe. The removed iron is magnetically compensated by an iron block added to the yoke in the vicinity of opening.

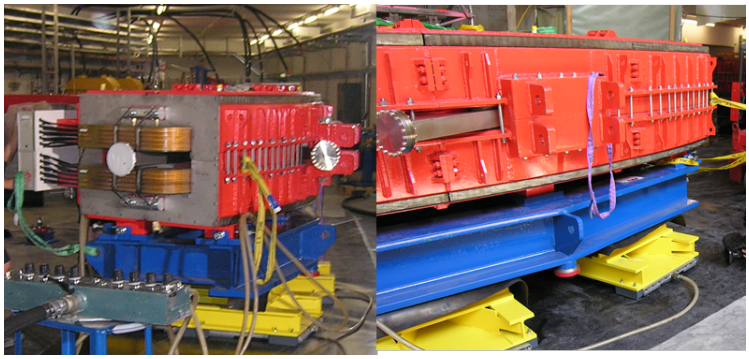

Fig. 27: The 45° HEBT dipole for the cancer therapy facility HIT in Heidelberg. The opening accommodating the straight beam pipe is magnetically compensated by an iron block (Photo C. Will, GSI Darmstadt).

Other examples for specially shaped yokes are the ones used in synchrotron light sources. The synchrotron light is tangentially emitted at the bends of the synchrotrons. Magnetic elements after the bends must not interfere with the beam lines for the synchrotron light. Therefore, special yoke shapes need to be used. Figure 28 shows as example a sextupole of the Australian Light Source.

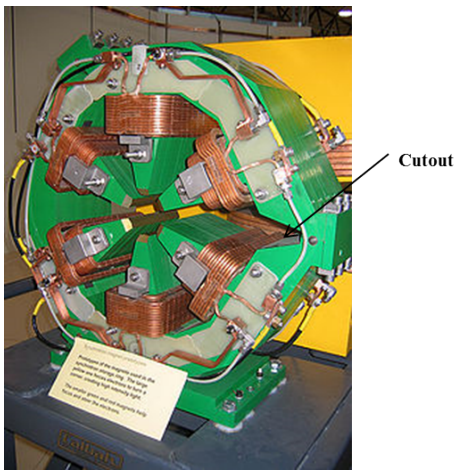

Fig. 28: Prototype sextupole for the storage ring of the Australian Light Source. Its yoke has a cut out at the right side to generate the clearance for the beam line [5].

6.4 Integrated magnets

Several different magnets can be integrated into one body for saving space or improving the overall stability.

The first example shows the corrector multipoles used in the SIS18 at GSI (Fig. 29). The longitudinal space is very limited. Therefore, three multipoles (normal quadrupole, skew quadrupole, and skew sextupole) are integrated into one body. All magnets are iron free. The saddle coils are arranged concentrically.

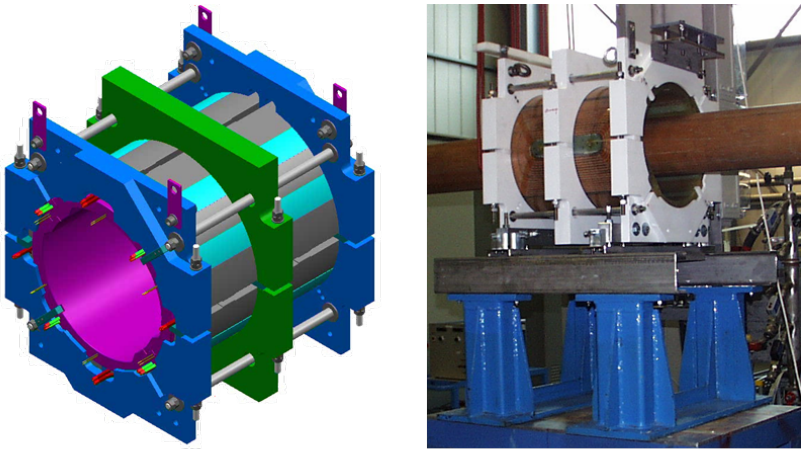

(a) (b)

Fig. 29: Corrector multipoles for SIS18 at GSI: (a) computer model of a correction magnet containing a normal quadrupoles, a skew quadrupole and a skew sextupole, (b) corrector multipole during testing. The brown tube inside the aperture contains the measurement coil.

Another example is the main magnets for the MAX IV storage ring in Lund (Fig. 30). The magnetic elements (e.g., one dipole, two quadrupoles, three sextupoles and two steering magnets) are integrated into a common yoke. The upper and the lower half of the yoke are precision machined iron blocks. The yoke itself acts as common girder for all magnets as well as for flux guidance. All magnetic elements are well aligned with respect to each other during the manufacturing process. Therefore, the alignment process of the machine itself is accelerated. The position of the magnetic elements within one main magnet is not influenced by ground settlements.

Fig. 30: Main magnet for MAX IV. This type (U1) contains one main dipole, two quadrupoles, three sextupoles. as well as *x*- and *y*-steering magnets [6].

6.5 Special yoke materials

As an example of special yoke materials, cobalt iron (CoFe) will be used here. By adding up to 50% Co to the yoke material, the saturation flux density can be increased to about 2.25 T. This enables compact design with high fields or field gradients. This advantage has to be paid for with a much higher price (up to 200 €/kg). Additionally, the manufacturing needs special care as the material is brittle. Also, care must be taken to avoid activation of Co during operation.

The examples show internal quadrupoles of an IH-type LINAC (seen in Fig. 31). The quadrupole yokes are made of 0.35 mm cobalt iron sheets. The pole base is enlarged to the maximum. Single layer coils are used. Gradients up to 124 T/m inside the 20 mm diameter aperture can be achieved. The quadrupole triplets are finally integrated into copper-plated drift tubes, which is another example for integrated magnets.

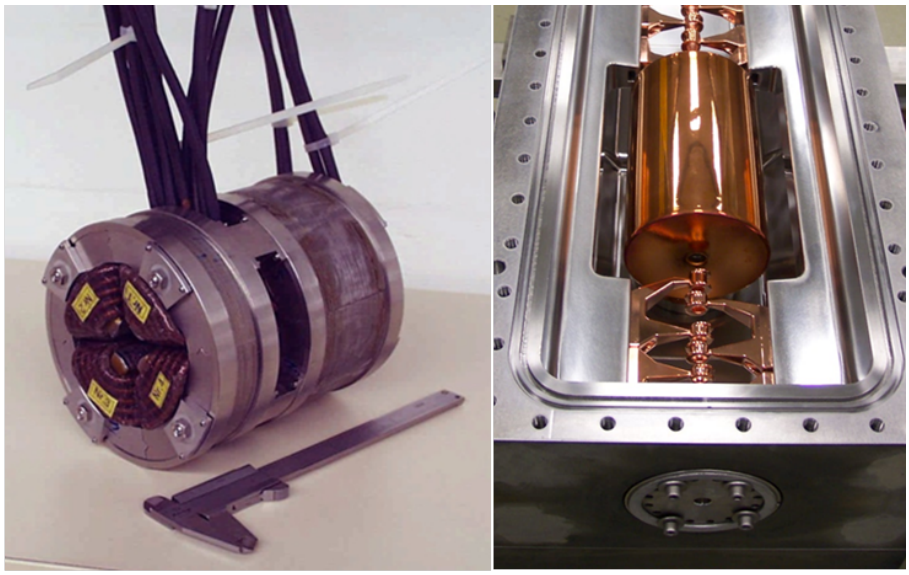

(a) **(b)**

Fig. 31: (a) Prototype quadrupole doublet for high field gradients with CoFe yoke, (b) fully integrated quadrupole triplet inside an IH-type LINAC.

6.6 Solenoids

In the simplest case, a helical winding represents a solenoid. The main field is parallel to the axis and for long solenoids the magnetic field inside is constant. In contrast to quadrupoles, a solenoid focusses both planes simultaneously. For explaining the focusing effect, both the main field and the stray field have to be taken into account. The stray field at the ends of the solenoid is radially oriented. A charged particle approaching the solenoid, experiences an azimuthal force due to the radial field. The created azimuthal motion causes the main field of the solenoid to produce a force that is directed towards the axis of the magnet. The charged particle beam is focused independently from the *x*- and *y*-plane.

Sizes vary from several tens of centimetres to several tens of metres (Fig. 32). Depending on the required focussing strengths, normal conducting or superconducting solenoids are used. Typical applications are low-energy beam lines in the vicinity of ion sources (mostly normal conducting), linear accelerators (often superconducting), and magnets for particle tracking in experiments (normal or super conducting).

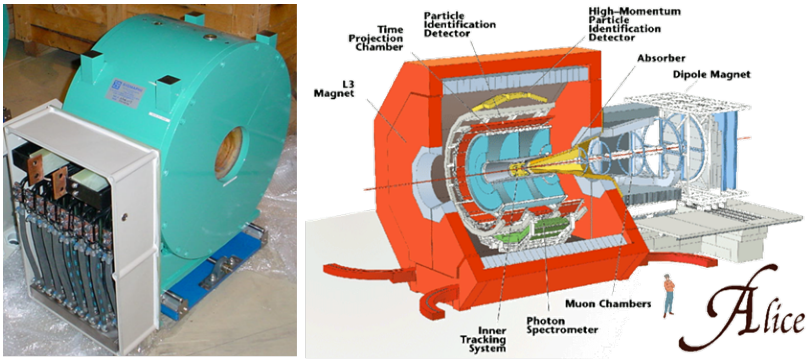

(a) (b)

Fig. 32: (a) The solenoid used in the low energy beam transfer line of the Cancer Therapy Facility in Heidelberg having a diameter of ~0.6m and a length ~0.3m, it weighs 0.5 t, (b) the central solenoid of Alice [7] is ~12 m in diameter and ~12 m in length. Its weight is ~10,000 t. Both magnets have central field of about 0.55 T.

6.7 Magnetic horns

A magnetic horn (or van der Meer horn) is a pulsed high-current focusing device. It is used to focus the secondary beam after a production target. The central path is free of magnetic field and matter. Therefore, the primary beam is not influenced and cannot damage the horn. Off-axis (secondary) particles are focused (shown in Fig. 33).

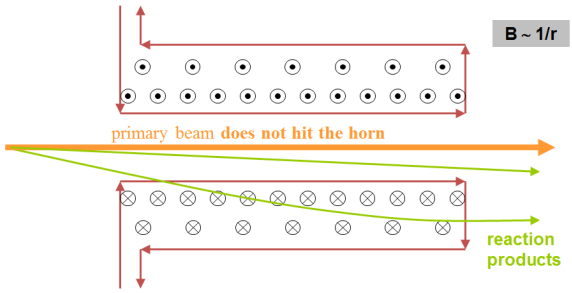

Fig. 33: Principle of a magnetic horn. A rotational magnetic field is generated by a single turn high current set up (fig. K. Knie, GSI Darmstadt).

A magnetic horn will be used in the pbar separator of the FAIR project to focus antiprotons (shown in Fig. 34). The planned operating data are 400 kA and 15 kV. The inner conductor of the horn is shaped in a way that a parallel antiproton beam is generated independent of its original angle to the axis.

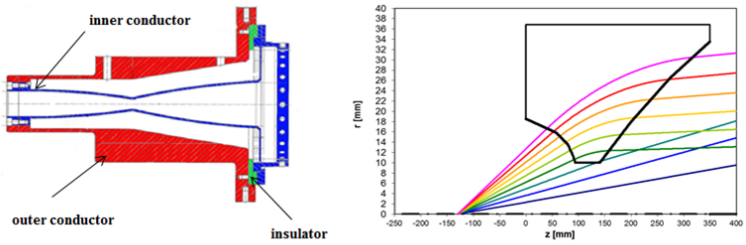

(a) (b)

Fig. 34: (a) Cross-section of the magnetic horn for the pbar separator at FAIR, (b) trajectories of antiprotons with different angles to the axis through the horn. A parallel beam is formed (figure K. Knie, GSI Darmstadt).

6.8 Toroids

Toroids exhibit a donut shaped magnetic field. The magnetic flux is closed and no distinguished poles exist. Outside the toroid, the stray field is weak.

The toroid magnet system of the High Acceptance Dielectron Spectrometer (HADES) at GSI consists of six super-conducting air coils (see Fig. 35). In a volume of 9 m^3 up to 3.6 T can be achieved. The space between the coils is to accommodate the different detector systems. They consist of more than 82,000 individual detectors.

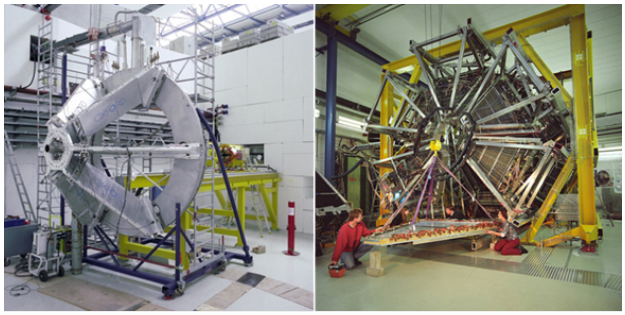

(a) (b)

Fig. 35: (a) The toroid magnet system of the HADES experiment at GSI. Six super-conducting air coils are integrated in the spokes, (b) installation of the detector systems into the toroid.

7 Examples

7.1 Cancer therapy facility HIT in Heidelberg

In this section, examples for magnets described above are depicted with the magnets designed and produced for the cancer therapy facility HIT in Heidelberg.

The HIT centre is a dedicated therapy facility for treating cancer tumours. It is the first of a kind facility in Europe to provide treatments using both protons and carbon ions. Another striking feature of the HIT is its ability to provide a 360° rotating beam for radiation therapy. The HIT facility was in general developed by the GSI Helmholtz Centre for Heavy Ion Research in Darmstadt with contributions from MT Aerospace and a co-operation between Siemens Healthcare and experts at HIT-Betriebs GmbH. The entire project was funded equally by the Heidelberg university hospital and by the German government. The centre has been treating patients since 2008. Being almost half the size of a soccer field, it encompasses a gigantic device (discussed shortly).

HIT has a footprint of approx. 70 m × 70 m. An overview of the facility can be seen in the Fig. 36. Being a compact accelerator, most magnet designs and features described above can be found here. For completeness, some magnetic septa are also shown.

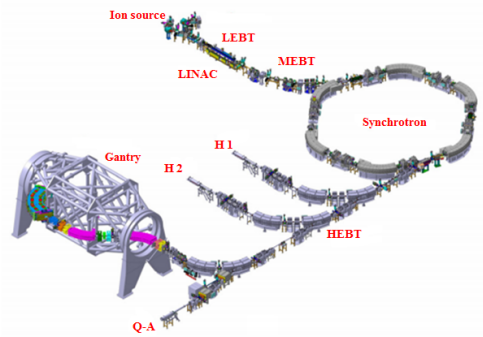

Fig. 36: Cancer therapy facility HIT [8]

The facility is equipped with two ion source branches. The electron cyclotron resonance ion sources produce light ions ranging up to oxygen. The magnets in the low energy beam transport (LEBT), guide the beam to the linear accelerator (LINAC). After the LINAC, the beam reaches an energy of 7 MeV/u which equals about 10% the speed of light. This is followed by a synchrotron with a circumference of about 65 m, where the beam attains at maximum approximately 73% the speed of light which equals a beam rigidity of 6.6 Tm. After the required energy is reached (please see Table 5), the beam is distributed by the HEBT to several beam lines. H1 and H2 are horizontal beam lines for patient treatments. The third branch guides the beam along an isocentric *gantry* (the gigantic device mentioned earlier). There also exists a fourth beam line for quality assurance (Q-A) and R&D purposes.

Table 5: Beam parameters for the HIT

Parameter	Protons	Light ions (e.g., carbon)
Energy	48-221 MeV/u	88-430 MeV/u

Aiming on a high reliability all magnets were designed conservatively. Wherever possible, existing designs and tooling were reused.

7.2 LEBT magnets

The ion beam is electrostatically extracted from the ion sources. Due to its low energy, it can by influenced by relatively small magnetic fields. This is visible in the design of the magnets in the LEBT.

At first the beam is focused by a solenoid already described in section 6.6.

The LEBT quadrupoles, one singlet before and one triplet behind the analysis dipole provide further focusing (see Fig. 37). Being low gradient (3.2 T/m) quadrupoles, these make use of the standard design type I for their yokes. The parallel sided poles are surrounded by a cylindrical coil. To minimize the crosstalk between the magnets, they are equipped with mirror plates.

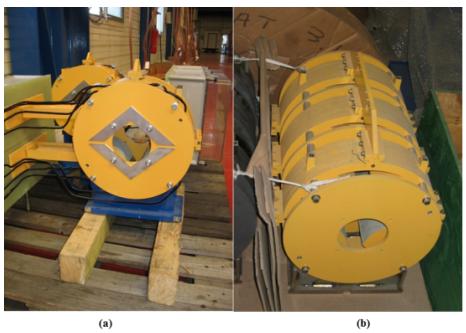

Fig. 37: (a) LEBT quadrupole singlet, (b) quadrupole triplet yoke

The analysis dipole is used for the magnetic separation of the charge state distribution delivered by the ion sources (shown in Fig. 38). It is an H-type dipole with a deflection angle of 90°. Due to the low energy, field (0.2 T) and bending radius are small (400 mm). A production using stamped laminations was geometrically impossible. Rough cut laminations were glued to a rigid block. The final yoke structure with one curved and one straight coil window was milled. The coil is D-shaped to avoid a negative curvature on the inside.

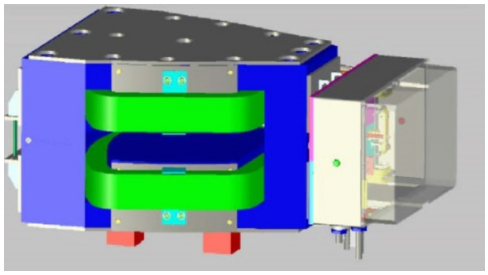

Fig. 38: Analysis dipole for charge separation behind the ion source

The switch yard dipole is used for funnelling the ion beams from the two ion sources to the linear accelerator (seen in Fig. 39). It is a simple, straight H-type dipole with a 0.1 T field.

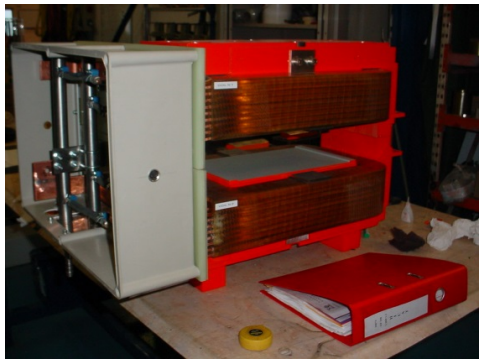

Fig. 39: Switch yard dipole

The LEBT is equipped with three pairs of combined horizontal/vertical LEBT steering magnets (Fig. 40). This allows the compensation of angular errors as well as axis offsets of the beam in both ion source branches and in front of the LINAC. The steering magnets have a window-frame design. The cylindrical coils are wound around the yoke. Due to the low field (0.0252 T), the power is low and no active cooling is required.

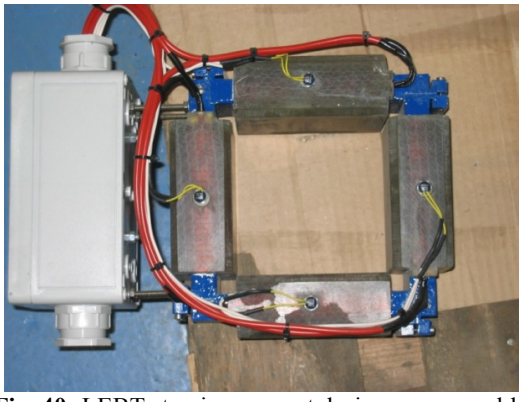

Fig. 40: LEBT steering magnet during pre-assembly

The focusing into the LINAC structure is done by another solenoid of the same type as described in section 6.6.

7.3 LINAC magnets

The LINAC consists of two radio frequency accelerating structures: one Radio Frequency Quadrupole (RFQ) tank and an Interdigital H-mode (IH) tank. The matching section between both tanks is

equipped with a quadrupole doublet. It makes use of the same quadrupoles as inside the IH-tank and directly behind the IH-tank. They were described in section 6.5.

The matching section contains in addition, a combined horizontal/vertical steering magnet (as in Fig. 41). To be as compact as possible it comprises a window-frame design with four single layered cylindrical coils and an extremely short yoke. It is integrated together with the quadrupole doublet into a stainless steel housing.

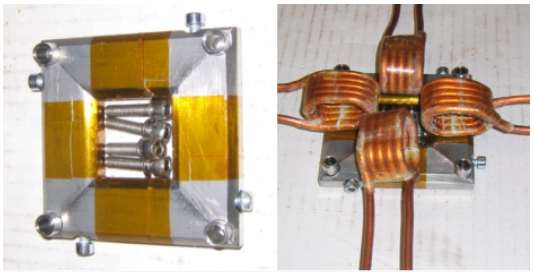

Fig. 41: Matching steering magnet: (a) pre-assembled yoke of the matching steering magnet, (b) yoke and coils during assembly preparation.

7.4 MEBT magnets

The MEBT provides the beam transport to the synchrotron as well as a so called stripping section. Lighter ions are stripped here to higher charge states (e.g., C^{3+} -> C^{6+}).

Two 25° dipoles bend the beam into the synchrotron injection channel and provide charge state separation after the stripper (shown in Fig. 42). A curved H-type design is used. The magnets were stacked from stamped laminations. Their field is 0.57 T.

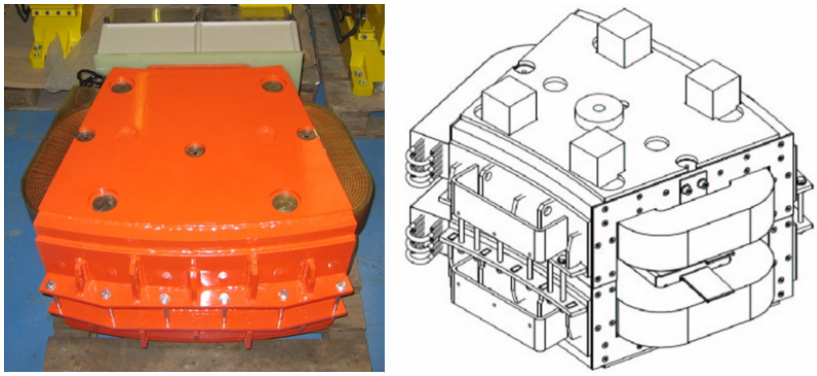

Fig. 42: MEBT dipole between linear accelerator and synchrotron

The quadrupoles in the MEBT make use of the same cross-section as the HEBT quadrupoles and are described with them in section 7.6.

The MEBT is equipped with horizontal/vertical steering magnets, too. A low cost design was intended during their original development at GSI in the 1970s. The stator of a standard electromotor is used as yoke. The coils have a $\cos\theta$ design. Cooling is provided indirectly by a radiator wrapped around the yoke (shown in Fig. 43).

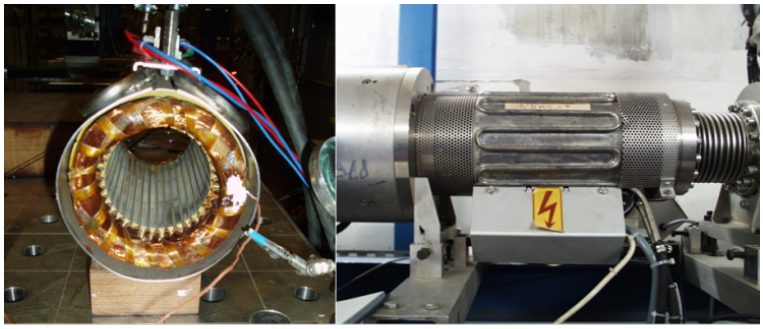

(a) (b)

Fig. 43: (a) Beam pipe steering magnet during test at GSI, (b) magnet integrated in a beam line

The injection into the synchrotron is provided by a curved window-frame C-dipole. It has a curved yoke (15°). The field is 0.42 T. The stray field on the circulating beam is reduced by a soft iron screen. This type of magnet is often called magnetic septum. In the Heidelberg case we called it a inflector dipole (shown in Fig. 44).

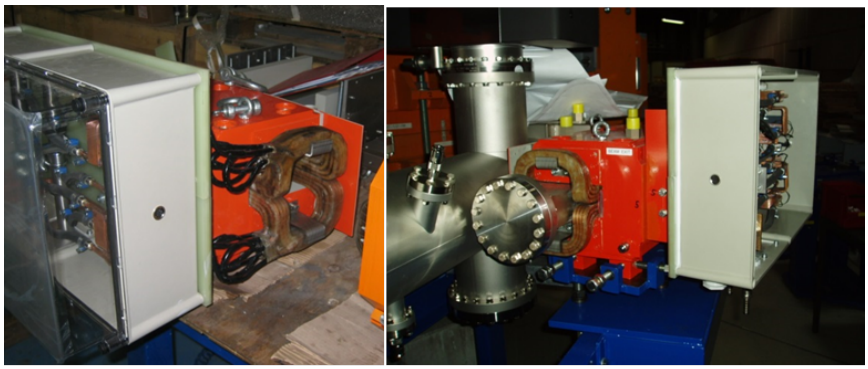

(a) (b)

Fig. 44: Inflector dipole into the synchrotron: (a) entrance of the inflector dipole, (b) exit of the inflector dipole during installation. To the left of the magnet, the beam line for the circulation beam can be seen.

7.5 Synchrotron magnets

The main dipoles of the synchrotron are H-type dipoles with a deflection angle of 60°. Three curved stacks are connected to the dipole to limit aperture reduction. All six dipoles are operated in series with one power supply. Therefore, magnet-to-magnet identity has to be taken care of. Removable end plates allow the adjustment of the magnetic length by insertion of additional laminations (see Fig. 45). The field is 1.53 T with a ramp rate of 1.53 T/s. Correction coils are integrated into the main coils to provide horizontal steering.

(a) (b)

Fig. 45: (a) Synchrotron dipole with 60° bending angle, (b) insertion of an additional lamination for adjusting the magnetic length.

The synchrotron quadrupole relies on a figure-of-eight design and has a gradient of 7 T/m. The yoke cross-section is identical to the quadrupoles in the synchrotron SIS18 at GSI. The coils were adapted from quadrupoles in the injection channel to SIS18. The twelve quadrupoles are operated with four power supplies having three quadrupoles in series each. As with the dipoles, magnet-to-magnet identity has to be taken care of. Removable end pieces (see Fig. 46) allow the adjustment of the magnetic length by insertion of additional laminations.

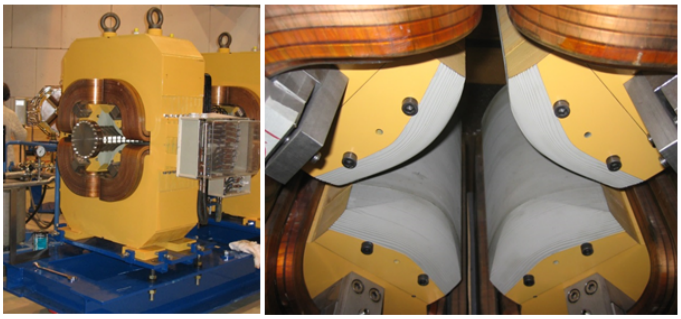

(a) (b)

Fig. 46: Synchrotron quadrupoles: (a) two synchrotron quadrupoles on a common girder during pre-assembly, (b) removable pole end pieces.

The sextupoles have a design similar to the standard quadrupole type II. The coils are cranked accordingly (seen in Fig. 47). The yoke consists of three parts, each containing two poles. The gradient amounts to $\frac{d^2B}{dx^2} = 26.7\ \mathrm{T/m^2}$. The cross-section of the yoke is identical to the sextupoles in SIS18, whereas a new coil design has been developed.

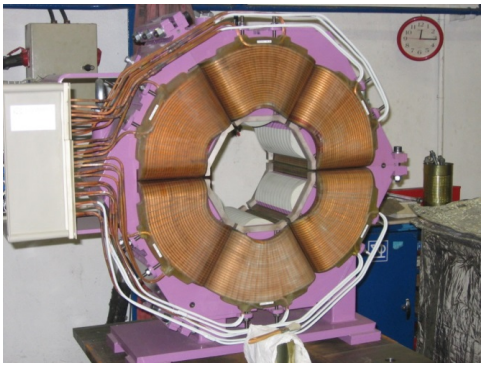

Fig. 47: Sextupole for the synchrotron during production

Vertical steering in the synchrotron is provided by window-frame design steering magnets with cylindrical coils. The field is 0.134 T. The field quality was improved by a spacer in the centre of the coils as seen in Fig. 48.

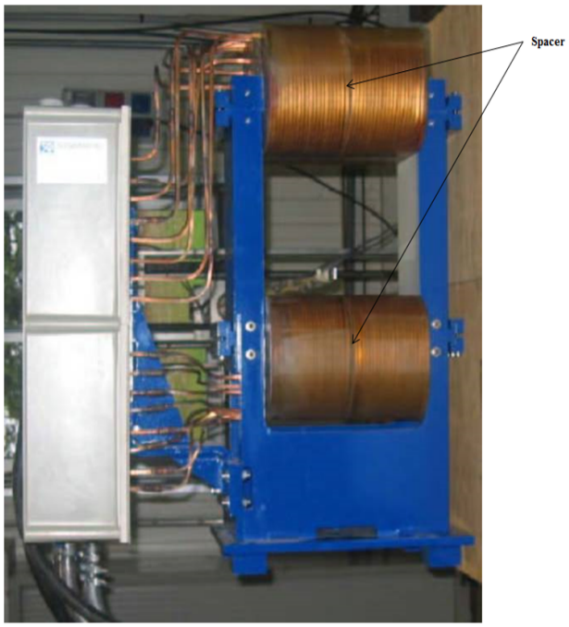

Fig. 48: Synchrotron vertical steering magnet during test

During injection, the beam must be stacked by very fast dipole magnets. For this purpose, the synchrotron is equipped with three so called bumpers (Fig. 49). These are two-turn window-frame dipoles. Because of the fast ramp rate (560 T/s), thin laminations are not sufficient for the suppression of eddy currents: The yokes are manufactured from powder composite materials. The absolute field level is small (0.0195 T).

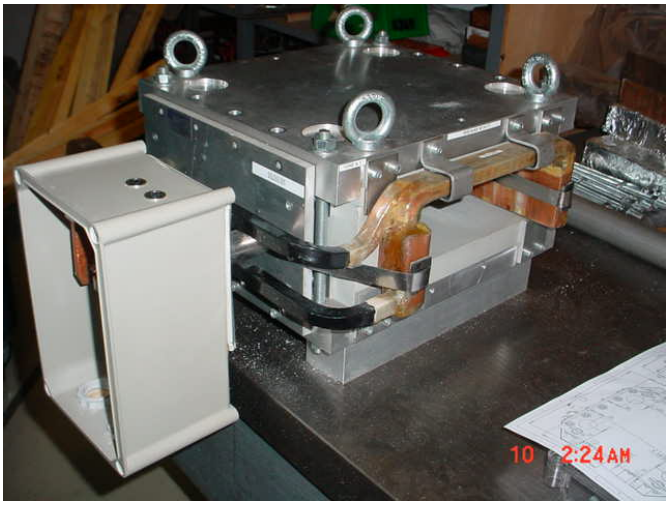

Fig. 49: Bumper magnet

The extraction channel is equipped with two magnetic septa.

The septum I is a straight window-frame dipole with C-shaped yoke. It has a deflection angle of 6.5°. To have enough horizontal space for the deflected beam, the gap widens after about two thirds of the magnet length (see Fig. 50). Coil and vacuum chamber are made accordingly. The coil is soldered from different copper parts for achieving tight bending radii and tolerances.

(a) **(b)**

Fig. 50: (a) Septum I seen from the circulating beam side, (b) vacuum chamber for Septum I. The lower branch is bent for the deflected beam.

Septum II is a curved window-frame dipole with a curved c-shape yoke (see Fig. 51). It has a deflection angle of 13.5° at 0.9 T. It is operated in series connection with the main dipoles of the synchrotron.

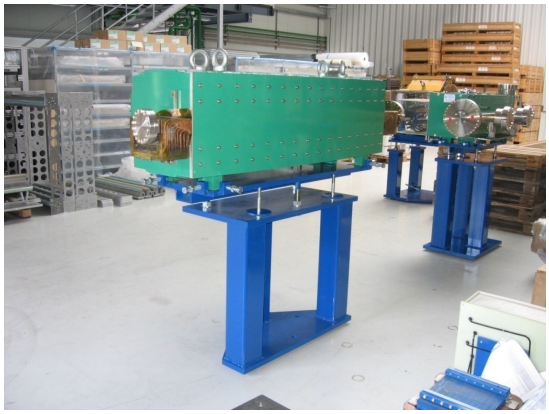

Fig. 51: Septum II

7.6 HEBT magnets

Directly after the synchrotron, the spill abortion bumper (as seen in Fig. 52) is located. In case of any failure it provides a fast switch off of the beam. Only if the magnet is switched on is the beam transported to the HEBT. If it is switched off, the beam is aborted into a dedicated beam dump. It is a fast magnet (1000 T/s) with only a few turns. The yoke is made of powder composite material. It has a deflection angle of 0.69° at 0.2 T.

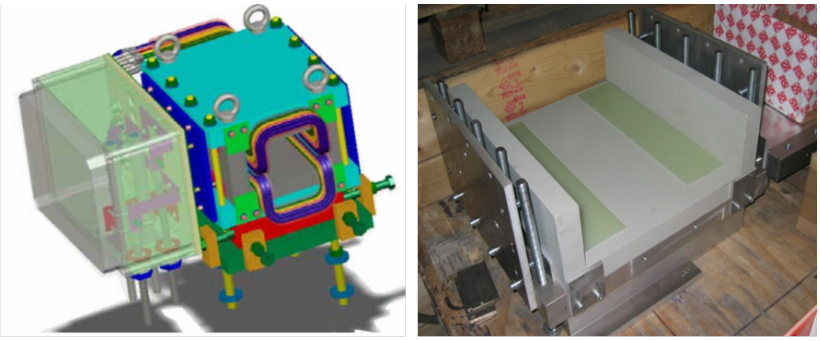

(a) (b)

Fig. 52: (a) Spill abortion bumper, (b) lower half-yoke spill abortion bumper. It is manufactured from powder composite material. The yoke parts are kept together by a stainless steel structure.

The 15° and 45° dipoles are used in the high energy transfer beam lines (shown in Fig. 53). They have identical cross-sections. They are curved H-type dipoles with a field of 1.51 T. Zero field correction coils are integrated into the main coils for the usage at branching points (see also section 6.3). The 45° dipoles are made from three stacks to limit the aperture reduction. The poles have a hole for the compensation of saturation effects (see also section 5.2).

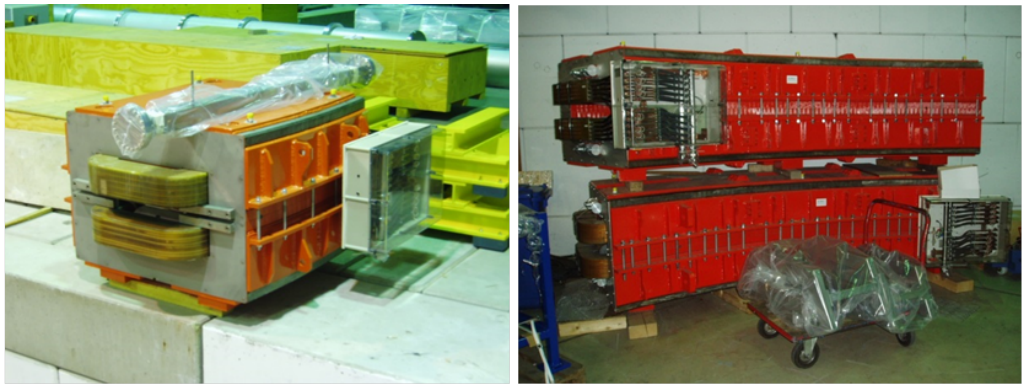

(a) **(b)**

Fig. 53: (a) The 15° HEBT dipole, (b) two 45° HEBT dipoles in storage

The quadrupoles in the HEBT, MEBT, and on the gantry make use of the same cross-section (depicted in Fig. 54). They are based on the standard design type II. The pole basis is enlarged to the maximum. The coils are cranked accordingly. The yoke lengths are adapted according to the requirements. The HEBT quadrupoles have a yoke length of 490 mm, whereas the MEBT and the gantry quadrupoles have a yoke length of 290 mm. The yoke cross-section and the coil design were copied from existing GSI beam line magnets.

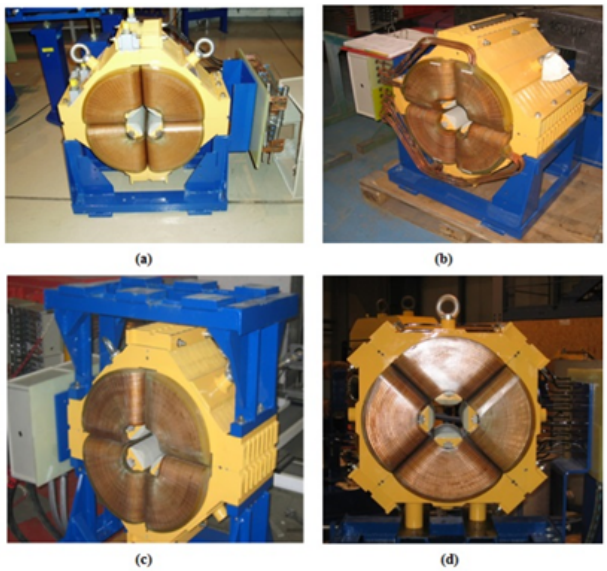

Fig. 54: MEBT, HEBT, and Gantry quadrupoles: (a) MEBT quadrupole (yoke length 290 mm), (b): HEBT quadrupole (yoke length 490 mm), (c) gantry quadrupole with top and bottom girder (yoke length 290 mm), and (d) skew quadrupole for matching section to gantry (yoke length 290 mm). The gradients for both lengths are similar. The shorter ones have 18.8 T/m and the longer ones 19.3 T/m.

Horizontal and vertical steering in the HEBT and on the gantry is provided by simple window-frame dipoles with cylindrical coil (seen in Fig. 55). Yoke and coils for horizontal and vertical steering magnets are identical. The field is 0.1 T.

Fig. 55: HEBT horizontal and vertical steering magnet

Each treatment area, as well as the Q-A area, is equipped with a horizontal and a vertical scanning dipole. They allow the scanning of the ion beam over the tumour cross-section as in a cathode ray tube. Apart from the interface to the girder, horizontal, and vertical scanning dipoles have an identical design. The fast ramped (62 T/s) straight window-frame dipole has a field of 0.31 T. Its lamination thickness is only 0.35 mm, whereas all other magnets have 1 mm laminations. To minimize the eddy current effects, the vacuum chamber is thin walled (0.35 mm). It is corrugated to withstand the atmospheric pressure.

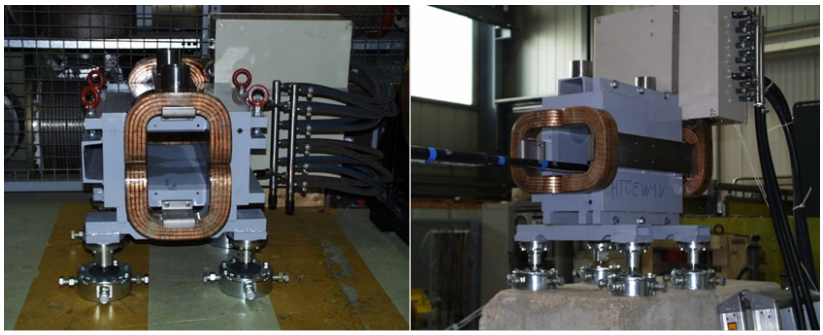

(a) (b)

Fig. 56: Scanning dipoles during tests at GSI: (a) horizontal scanning dipole (GSI), (b) vertical scanning dipole

7.7 Gantry

While the treatment areas H1 and H2 deliver the ion beam horizontally, a gantry on the other hand allows the rotation of the beam around the patient. The patient is located in the isocentre. The beam line, including all necessary infrastructures, is rotated around the patient. A sketch of a so-called isocentric gantry is shown in Fig. 57.

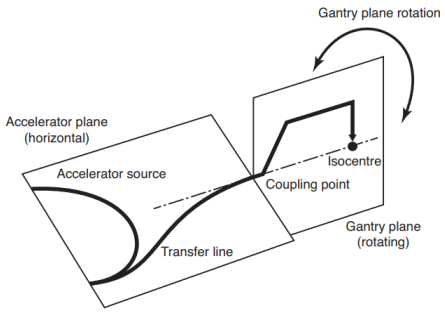

Fig. 57: Principle of an isocentric gantry [9]

With the isocentre, it is implied that the focal point is the same at every position for any rotational angle of the gantry. This eliminates the need for a patient lying on the isocentric axis to be moved vertically, with the gantry rotating horizontally. Another advantage of the gantry is that it has a large good field region.

The size of a gantry is solely determined by the use of normal conducting dipole magnets. These are not only used to transport the beam along the axis. They are additionally used to create an offset between the beam axis and the gantry's rotational axis and to further bend the beam towards the patient lying on the isocentric axis.

As may be recalled from section 5.2, the saturation of iron already starts at 1.5 T, thus restricting the maximum field on the beam axis to less than 2 T (approximately 1.8 T). Considering the beam rigidity of protons at the required energy, as in Table 5 with a field of 1.8 T, the gantry must have a radius of at least 5 to 6 metres, making it huge.

At HIT, as both protons and heavy ions are used and the gantry is significantly larger than conventional ones. With a maximum energy of 425 MeV/u and a rigidity of 6.57 Tm, a bending radius of 3.65 m is reached. With the normal conducting dipole technology, it results in a gantry of size ≈ 19 m in length and ≈ 15 m in diameter spanning up to 3 floors in height. The overall mass is 600 tonnes, 135 tonnes of which are contributed by the magnets that guide the beam to the gantry. Despite its huge rotating mass, a positioning accuracy of about ± 0.5 mm about the tumour is achieved (which is comparable with a proton gantry).

All magnets on the gantry are equipped with girders and alignment feet on the top and at the bottom. By these means, they are restrained inside the gantry structure and the required accuracy can be achieved.

As describe above, the gantry diameter is determined by the dipole field level. To keep the gantry compact, all dipoles on the gantry have a field of 1.81 T. Two 45° dipoles generate the necessary offset distance from the rotational axis (see Fig. 58). They are curved hybrid design dipoles: an H-type yoke is equipped with an additional inner bedstead coil between the poles. The outer coil is of bedstead type too. The yokes are made from two stacks to limit aperture reduction.

Fig. 58: A 45° gantry dipole during pre-assembly

The last magnet is the 90° gantry dipole. It has a window-frame design. It is the magnet with the largest aperture in the facility as it has to accommodate the scanning magnet's deflected beam. The curved yokes are made from three stacks to limit the aperture reduction (shown in Fig. 59). Holes beside the poles limit the influence of saturation (see section 5.2).

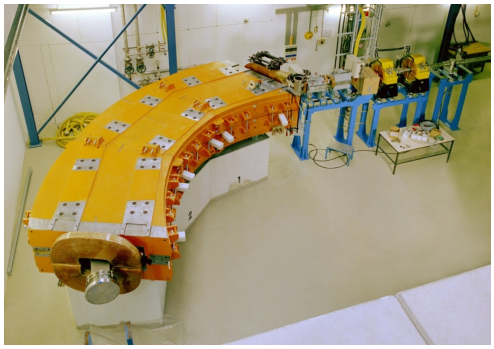

Fig. 59: The 90° gantry dipole during test at GSI

The quadrupoles, steering magnets, and scanning magnets on the gantry are, with the exception of the girders, identical to the HEBT magnets, which are described in section 7.6.

8 Acknowledgements

The author wishes to acknowledge support from numerous colleagues inside and outside GSI, especially from V. Srinivasan and P. Rottländer.

References

[1] J. Franklin, *Classical Electromagnetism*, (Dover Publications, New York, 2017).

[2] J. Tanabe, Iron Dominated Electromagnet Design, US Particle Accelerator School, June 2005, SLAC-R-754, http://www.slac.stanford.edu/cgi-wrap/getdoc/slac-r-754.pdf.

[3] http://www.luvata.com/.

[4] G. Schnell, *Magnete Grundlagen - Aufbau- Anwendungen*, (Verlag Karl-Themig München, 1973).

[5] https://commons.wikimedia.org/wiki/File:Aust.-Synchrotron,-Sextupole-Focusing-Magnet,-14.06.2007.jpg.

[6] M. Johannson, Beam Dynamics meets Magnets- II workshop, Bad Zurzach, 1−4 Dec 2014.

[7] https://cms.cern/detector/bending-particles

[8] D. Ondreka and U. Weinrich, GSI, Darmstadt, Germany, 'The Heidelberg ion therapy (HIT) accelerator coming into operation', Conf.Proc. C0806233 (2008) TUOCG01

[9] H. Owen et al., Technologies for delivery of proton and ion beams for radiotherapy, arXiv:1310.0237

Bibliography

Proceedings of the CAS-CERN Accelerator School: Magnets, Bruges, Belgium, 16-25 June 2009, edited by D. Brandt, CERN-2010-004, http://cdsweb.cern.ch/record/1158462.

Proceedings of the CAS-CERN Accelerator School: Measurement and alignment of Accelerator and Detector Magnets, Anacapri, Italy, 11-17 April 1997, edited by S. Turner, CERN-98-05, http://cds.cern.ch/record/318977

J.T. Tanabe, *Iron Dominated Electromagnets*, (World Scientific Publishing Co., 2005), https://doi.org/10.1142/5823.

IEEE, Proceedings of International Conferences on Magnet Technology, every 2nd year, e.g., 24th International Conference on Magnet Technology (MT-24), Seoul, 2015 [IEEE Trans. Appl. Supercond. 26 (2016) no. 4].

H.E. Knoepfel, *Magnetic Fields* (Wiley and Sons, New York, 2000).